applied sciences

MDPI

Article

Detection of Pest Feeding Traces on Industrial Wood Surfaces with 3D Imaging

Andrzej Sioma [1,*], Keiko Nagashima [2], Bartosz Lenty [1], Arkadiusz Hebda [1], Yasutaka Nakata [2] and Kiichi Harada [2]

[1] Faculty of Mechanical Engineering and Robotics, AGH University of Krakow, al. Mickiewicza 30, 30-059 Krakow, Poland; hebdaa@student.agh.edu.pl (A.H.)
[2] Forest Management Laboratory, Graduate School of Life and Environmental Science, Kyoto Prefectural University, Kioto 606-0823, Japan; nagakei@kpu.ac.jp (K.N.); nakata-yasutaka@kpu.ac.jp (Y.N.); kiichi_0824@yahoo.co.jp (K.H.)
* Correspondence: sioma@agh.edu.pl

Featured Application: This research and its associated results from the technical solution can be used in wood quality control systems, flow-through imaging of wood surfaces, and real-time defect detection on production lines.

Abstract: This paper presents a method for detecting holes and grooves made by wood-boring pests. As part of the production process automation, wood delivered from sawmills is checked for defects visible on its surface. One of the critical defects that disqualifies wood from further processing is the presence of feeding marks left by various types of pests on its surface. This paper proposes a method for detecting this type of damage based on analysis of three-dimensional images of the wood surface. Three-dimensional imaging methods and the image resolutions resulting from the adopted imaging system's configurations are discussed. An analysis of the advantages and disadvantages of the methods investigated is presented, together with an assessment of their potential use in the implementation of the assigned control task, i.e., the detection of holes and grooves made by pests. Three-dimensional image parameters and interferences affecting the quality of the recorded image are described, along with the designed algorithm for identifying holes and grooves and the parametric description of the identified defect. The imaging effects for selected surfaces bearing signs of pest damage and the parameters describing the effectiveness of the present industrial solution are also presented. This paper demonstrates that it is possible to build a three-dimensional image to identify damage effectively within a minimum diameter of 1mm. It makes it possible to observe the damage carried out by most wood-boring pests.

Keywords: wood; wood-boring pests; surface defects; 3D image; image analysis; surface quality control

Citation: Sioma, A.; Nagashima, K.; Lenty, B.; Hebda, A.; Nakata, Y.; Harada, K. Detection of Pest Feeding Traces on Industrial Wood Surfaces with 3D Imaging. *Appl. Sci.* **2024**, *14*, 10775. https://doi.org/10.3390/app142310775

Academic Editor: Wilma Polini

Received: 2 October 2024
Revised: 12 November 2024
Accepted: 16 November 2024
Published: 21 November 2024

1. Introduction

Industries that use wood in various forms rely on material supplied from sawmills. One of the tasks associated with production automation is the control of parameters describing the quality of the provided material, and special attention is paid to detecting defects occurring on the material surface, which fall into three groups. The first group refers to the natural defects resulting from knots, colouring, or internal cracks. Another group results from incorrect mechanical processing and is identified by the presence of bark, machining marks, or dimensional flaws. The third group appears as visible traces of pests feeding, seen on the surface of the wood in the form of grooves and holes. These defects usually disqualify the wood from being processed in most industrial applications.

The shape and dimensions of the wormholes depend on the pest species infesting the wood. Some pests that develop during tree growth are referred to in the literature

as physiological-technical pests [1–3]. Pests invading the wood in woodpiles can cause technical damage [4]. The shape and size of wormholes are crucial factors for selecting control system parameters to detect their presence. By analysing the depth of the holes made by pests, it is possible to distinguish between three subgroups of surface defects, described as surface wormholes.

The first subgroup describes shallow wormholes that extend up to 2 mm into the wood. This damage is mainly caused by bark beetles, which are physiological pests that do not attack processed wood. If trees damaged by bark beetles are felled early, the resulting timber will retain its total value. An exception to this is the lesser pine shoot beetle (Latin: *Tomicus minor*). This species is responsible for causing the growth of a 'blue stain' fungus, which causes wood defects seen as black–grey patches in various tree species.

The second subgroup describes shallow wormholes extending up to 50 mm into the wood. The sawing process smooths out some of the wormholes, but some remain in the plank. This type of machining results in a loss of width in the sawn material. With circumferential cutting, the pest damage is transferred to the veneer, extracted from the wood's peripheral parts. For this reason, wormholes are classified as a technical defect.

The third subgroup contains defects referred to as deep wormholes. These defects are deeper than 50 mm and do not disappear during processing. They remain in the material made from round wood. Such signs of wood boring eliminate or drastically reduce the usability of the wood for technical purposes, including construction and furniture manufacture.

Besides the depth of the wormholes, other crucial factors include their dimensions, i.e., the hole diameter or the length of the groove visible on the material surface. These dimensions also depend on the species of pest inhabiting the wood, making it possible to distinguish between two groups of holes. The first group consists of round holes up to 3 mm in diameter. An entire life cycle of small wood-boring pests can occur in wood stockpiles. These pests can also feed on finished products and sawn timber. This damage, characterised by the small size of the hole, occurs in large numbers and often leads to the total decay of the wood. The second group of holes are large round or oval holes with a diameter of more than 3 mm. The pests that leave these type of holes are mainly forest dwellers, and the number of holes they make is smaller than that of the first group. These large, deep, but mostly isolated wormholes are easily removed during woodworking. Because of the size and visibility of the wormholes, the most common way to remove the damaged material is during the sawing process.

The analysis of the environmental conditions and factors that favour the development of different types of pests is not the subject of this paper. Instead, this paper focuses on analysing visible defects in the form of wormholes that occur on the surface of materials supplied by sawmills. The surface of round timber contains several different types of defects, including visible wormholes that pests create after cutting. These wormholes can be divided into two groups. The first group is represented by vertical wormholes that penetrate deep into the material, defined as holes more than 2 mm deep. The second group consists of horizontal wormholes which run parallel to the surface of the wood and are up to 2 mm deep.

Analysis of the pest damage observed on the surface of the boards during the preliminary research showed that 95% of the damage was visible in the form of holes up to 3 mm in diameter and 10 mm or more in length, filled with excrement left by wood-boring pests (Figure 1). This defect analysis was carried out on material graded by operators on dozens of batches of material supplied by different sawmills. Figure 1 shows the surface of the wood with wormholes of various shapes made by the pests. Magnified images of selected wormholes are also included in Figure 1. These images were obtained using a metrological glass scale with a millimetre grid marked on it. This tool was placed directly onto the surface of the wood containing the wormhole. The image was recorded using a stereovision microscope, which allows the shape of the wormhole to be observed with a

visible scale and enables the diameter and horizontal dimensions of each wood surface defect to be measured directly.

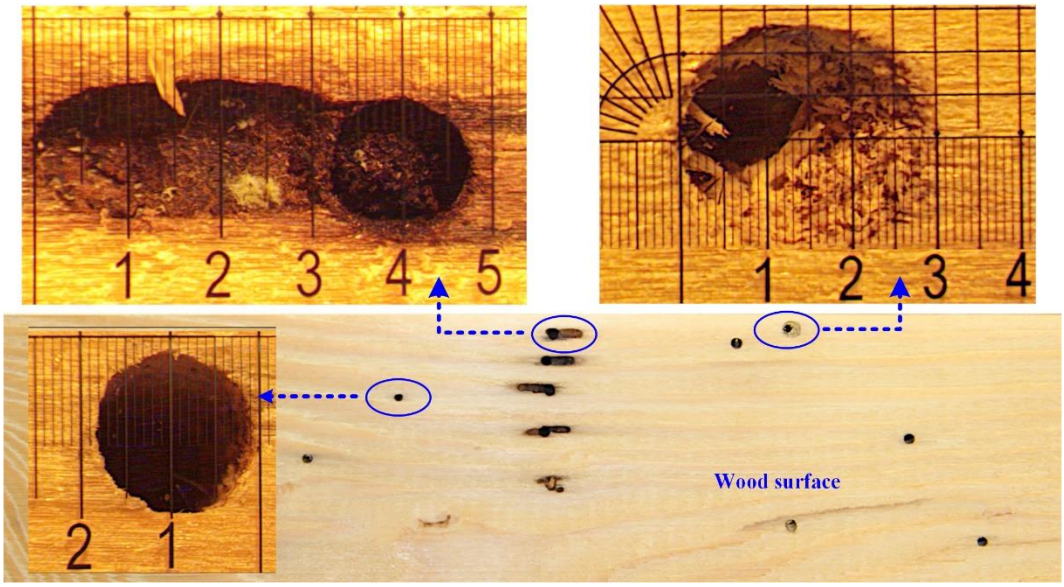

Figure 1. Examples of pest-caused holes on the wood surface analysed using a metrological glass scale with a millimetre grid.

The imaging of wood defects using vision systems has been developed over many years [5–7]. The majority of these systems use 2D imaging in the visible and infrared regions [8,9]. These images are used to analyse the wood surface and detect knots, cracks, and surface defects using conventional methods [10]. Fuzzy analysis methods are also used to analyse 2D images [11]. In recent years, image analysis methods based on artificial intelligence for wood defect identification tasks have also developed rapidly [12–16]. Thermography methods have also been investigated in wood inspection tasks [17,18]. Thermographic imaging is carried out at much lower resolutions [19]. One study [20] demonstrates the possibility of using microwave imaging to detect the presence of resin streaks in the log, but without being able to determine the location of the defect. There have also been successful attempts to use ultrasonic methods to detect wood defects in the form of cracks and the presence of knots [21]. Laboratory studies on the detection of pest larvae and wormholes using ultrasound are described in Fleming [22]. The authors confirm the possibility of detecting pest larvae in one-inch boards. Another approach is multi-sensor point analysis, which allows log validation in a selected cross-section [23]. Internal defects in wood are also analysed using computed tomography [24]. In the work of Choi [25] and McLoughlin [26], the authors used CT scanning to observe pests, including bark beetles, and to analyse the distribution of holes in logs. It is also possible to detect cracks, cavities, and foreign objects [27].

The use of computed tomography (CT) scans for planning the cutting of logs into boards has been the subject of intensive research. CT makes it possible to gather information on the position of knots in the log, which helps operators plan how to cut the boards [28–31]. Using three-dimensional imaging to detect pitch and measure annual growth is also possible [32]. The medical CT scanner also provides information on the density distribution in the log associated with uneven annual growth or wood moisture distribution [33–35]. Another application is determining the heartwood/sapwood boundary in the log [36,37]. Using CT in industrial applications allows imaging at a lower resolution than medical scanners [38]. It limits the detection capabilities of measurement systems based on this imaging technology.

Several papers [39–41] demonstrate the possibility of increasing the efficiency of plank production by using CT scanning to plan log sawing. One study [42] indicates an increase

in production efficiency of 23% for jack pine and 15% for white spruce. The return on investment is estimated to be around eight years for medium sawmills [43]. Operator safety is also an essential consideration for a system based on the CT method [44].

To date, applications of laser triangulation imaging in the timber industry have been limited to imaging the outside of the log before sawing [45]. Ondrejka et al. [46] compare the methods presented in terms of system cost and capability. The laser triangulation method (LTM) cannot image the interior of the material. It is also possible to propose a hybrid system combining 2D and 3D analysis capabilities [47].

According to an analysis of the literature, each method has certain drawbacks. The plane images obtained using visible light are susceptible to changes in intensity due to changes in the wood colour, its moisture content, and differences in surface treatment. Thermographic imaging suffers from low resolution and long exposure times. Furthermore, computed tomography and ultrasound imaging have significantly higher costs and require safety-critical working conditions.

The research described in this paper aims to prepare an automated system for detecting pest-feeding traces visible on the surface of wood in the form of wormholes for use in industrial conditions. It was assumed that the system should be able to detect wormholes on material transported at speeds of up to 1.5 m/s and that the inspection system should detect holes with a minimum diameter of 1 mm randomly distributed on the surface of the wood. However, the latter proved to be a redundant assumption because, during the preliminary research, holes with a minimum diameter of approximately 1.8 mm were detected on the wood surface (Figure 1). Nevertheless, this approach allows for the imaging of wormholes that are not closed during the wood surface treatment. It was also assumed that the imaging method and its parameters would be selected so that the system would not be sensitive to changes in the colour and moisture content of the wood. On the surface of wood with a high moisture content, the image of the wormholes should be similar to that of the regular material. A similar phenomenon occurs with wood that is darker in colour or wormholes that form close to the annual rings. Due to the industrial purpose of the system, it was assumed that the image acquisition and analysis should be at most 1 s. During this time, all wormholes visible on the wood surface should be identified and highlighted.

Quality assessment requires selecting the imaging method, resolution, and frequency [48]. These parameters should ensure that an image is produced that shows the wormholes as the material moves. The hole should be visible so that its diameter can be determined. Algorithms should then be proposed to identify the holes and their locations and to classify the material according to accepted quality criteria applicable to the production plant.

A triangulation method using line laser illumination was chosen for imaging the wood surface in this study. The technique produces a 3D image of the surface of the object. The scanning is carried out optically and is contactless so that the object remains intact after its evaluation. The technology is widely used in the woodworking industry and other industries. Jiang [49] proposed a method for the acquisition and analysis of 3D morphologies of coarse aggregates based on laser scanning. Other work [50] indicates the possibility of flatness deviation measurements of the aluminium body. The time needed for full-image analysis is up to 1000 ms. Another study proposed a configuration with two lasers of different wavelengths [51]. The authors evaluated the method in the case of printed elements and mushrooms. Hauck [52] developed a rail-track inspection system based on the LTM. It allows for non-contact range measurements and defect detection. Another case study that demonstrates the feasibility of the LTM is welding. This work [53] shows a lab-scale inspection system for detecting and classifying welding defects. The study considers five kinds of defects: surface cavity, pore, hump, burn-through, and lack-of-braze.

In the LTM, the laser line is used to determine the height profile, which is a set of points describing the height of a surface along a line. The laser provides reproducible illumination regardless of varying external lighting conditions. The colour of the wood does not affect the recorded 3D image of the surface. In addition, a change in the moisture content of the

wood does not affect the registered image. The surface analysis uses the coordinates of points (point clouds) distributed uniformly over the surface. A significant advantage of this imaging method is that it allows the surface image to be registered independently of the wood species. The imaging resolution parameters are given in the description of the triangulation method. Image analysis was carried out using an algorithm that allows for the location and evaluation of defects.

2. Materials and Methods

Based on an analysis of the imaging methods performed according to the assumptions, a decision was made to use three-dimensional imaging. This type of imaging makes it possible to describe a surface using measuring points described by three coordinates. The coordinates (x, y) described the point position, and the coordinate (z) defined the point height, which formed at the surface of the wood. It was assumed that the control system would operate in high-performance industrial conditions, which require the imaging of semi-finished wood products being transported at speeds of 1 m/s or more. The product should not be stopped at the inspection station, as this would reduce productivity. As a result of this approach, the LTM was chosen to image the wood surface. This method uses a laser line light to illuminate the wood surface. Using lasers operating in the 600–900 nm range allows constant surface illumination and registers a reproducible surface image regardless of the surface colour [54].

The conveyor systems of the machine moved the inspected boards in relation to the stationary vision system (Figure 2). A rotary encoder installed in the machine transmission system was responsible for synchronising the triggering of the acquisition of the 3D image of the wood surface. The method of illuminating the wood surface with the laser line is shown in Figure 2. The laser emits electromagnetic radiation with a wavelength of 658 nm and a power of P = 20 mW. The image of the laser line was recorded at a frequency depending on the acquired imaging resolution in the Y-axis direction. It was assumed that a circular image of the wormhole could have a diameter of not less than 1 mm. This research used a sensor with a resolution of 1536 × 512 pixels. The field of view for the vision system was set to FOVx = 175 mm. This field is projected onto the sensor and imaged onto 1400 pixels. It gives an image resolution of 0.125 mm/pixel in the X-axis aligned along the laser line, according to the following formula:

$$\Delta X = 175 \text{ mm}/1400 \text{ pixel} = 0.125 \text{ [mm/pixel]}. \quad (1)$$

The Y-axis resolution is set so that the distribution of points on the surface forms squares of the size defined by the X-axis resolution. In this case, the distances between points on the surface along the X-axis and the Y-axis are defined according to the formula:

$$\Delta Y = \Delta X = 0.125 \text{ [mm/pixel]}. \quad (2)$$

The resolution in the Z-axis depends on the chosen vision system geometry and the relative orientation of the camera and the plane formed by the laser beam. For the vision system geometry selected for the task (Figure 2), the Z-axis resolutions were determined using the formula:

$$\Delta Z = \Delta X/\sin(\alpha) = 0.125/\sin(45^\circ) = 0.18 \text{ [mm]}, \quad (3)$$

where:

ΔX—resolution along the X-axis direction, i.e., along the laser line;
ΔY—resolution along the Y-axis direction, assuming that ΔX = ΔY;
ΔZ—resolution along the Z-axis direction;
α—angle between the optical axis of the camera and the plane of the laser beam.

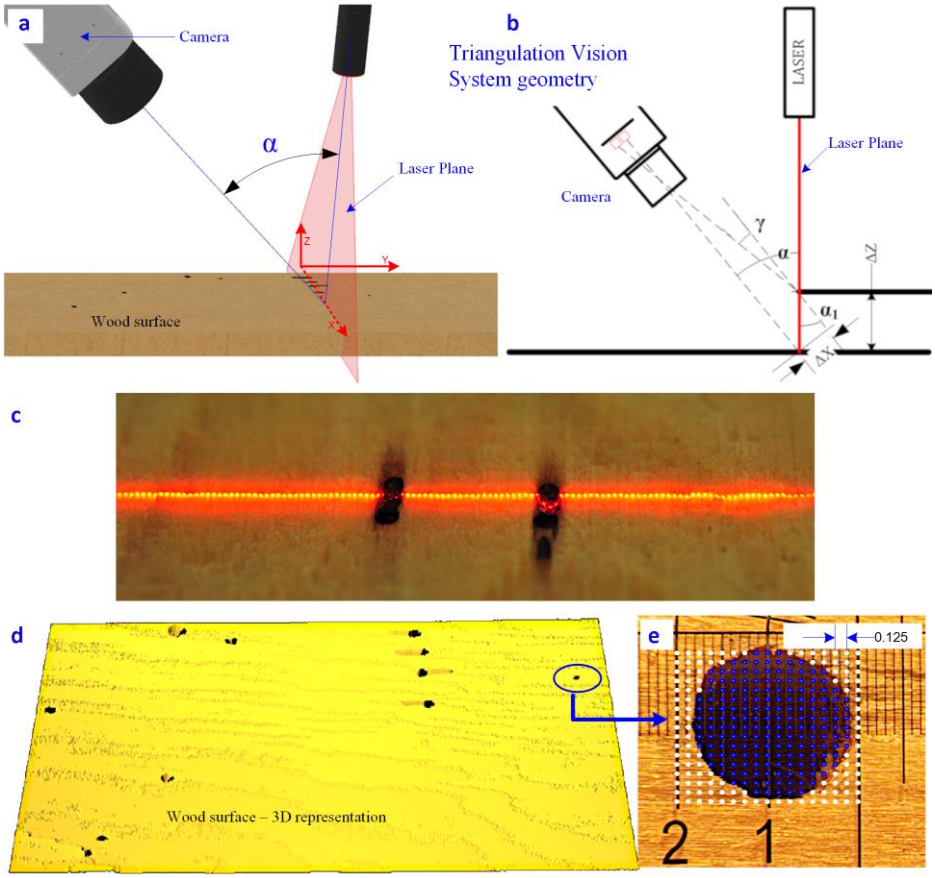

Figure 2. The 3D imaging method involved the following steps: (**a**) camera and laser alignment in relation to the surface imaged on the inspection station; (**b**) description of the geometry of the laser and camera setting for imaging in the LTM system; (**c**) view of the laser line projected on the wood surface' (**d**) three-dimensional image of the wood surface; and (**e**) distribution of measurement points (imaging with resolution 0.125 mm/pixel).

Figure 2 describes the method of recording the 3D images using laser triangulation. Figure 2b illustrates the working geometry of the laser and the camera that captures the images. The angular position between the laser plane and the camera's optical axis is also shown. This angle has a direct effect on the image resolution in the Z-axis.

During the operation of the conveyor belt, consecutive laser images were recorded on the surface of the wood. The laser image was acquired after the object movement by 0.125 mm was related to the resolution in the Y-axis (ΔY). For each image, a height profile was determined by describing the cross-section of the assessed material in a location illuminated by the laser line.

The position and shape of the laser line in the image defined the heights of the points that made up the imaged surface (Figure 2c). The position of the centre of the laser line was determined to establish the z-coordinate of the points. It was calculated for each point along the laser line (X-axis).

The 3D image was built by assembling a series of height profiles determined in the laser plane (XZ plane) for successive positions of the laser lines on the material. The image built using this method was composed of a cloud of points spread over the surface of the wood with ΔX and ΔY resolution. The height of each of these points was determined with a resolution of ΔZ.

During the analysis of the laser line image and the determination of the height profile points, an analysis of the intensity distribution in the cross-section of the laser line was used. This was the first image analysis operation to filter out noise on the wood surface.

The imaging resolution in the X- and Y-axes can be adjusted to reduce the number of points to be analysed or reduce the imaging time. However, reducing the number of points had a negative effect; the image of wormholes was represented by a smaller number of measuring points, which reduced the visibility of such defects on the surface. Four different values of the resolution $\Delta X = \Delta Y = (0.125; 0.20; 0.25; 0.5)$ were investigated in the preliminary research. Figure 3a shows the laser line projected onto the wood surface. The laser line scatters and refracts in the wormholes. It is visible in the form of its discontinuities (Figure 3a).

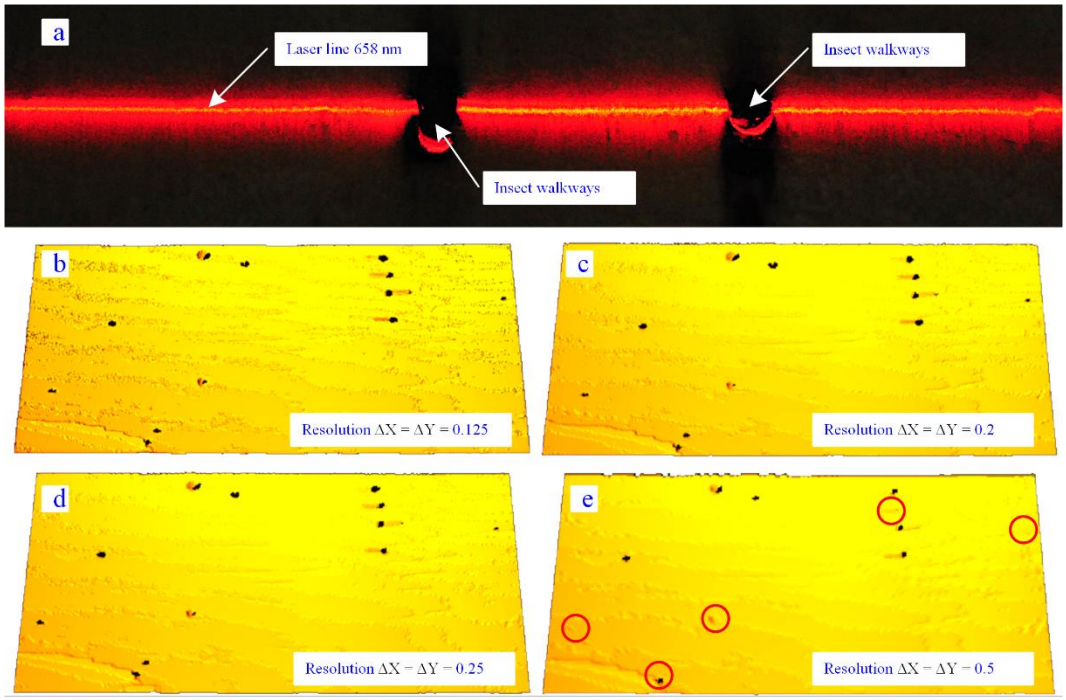

Figure 3. 3D images acquired with different resolutions, as follows: (**a**) image of the laser line on the wood surface used for profile generation—height profile is calculated based on laser line position in each column; (**b**) image acquired with a resolution of 0.125 mm/pixel (fully visible hole areas); (**c**) image acquired with a resolution of 0.2 mm/pixel; (**d**) image acquired with a resolution of 0.25 mm/pixel; and (**e**) image acquired with a resolution of 0.5 mm/pixel (some holes missing due to low resolution).

The imaging results showed that the images acquired with a resolution of $\Delta X = \Delta Y = 0.125$ gave a good representation of the holes and the micro-roughness on the surface of the wood (Figure 3b). An area of 1 mm^2 is described by 64 pixels in this image. The image recorded with a resolution of $\Delta X = \Delta Y = 0.2$ mm uses 25 points to describe an area of 1 mm^2 and sufficiently represents defects in the form of wormholes visible on the wood (Figure 3c). The visibility of these defects already decreases at a resolution of 0.25 mm, where an area of 1 mm^2 is described by 16 points (Figure 3d). The visibility of the defects decreased significantly in images acquired at a resolution of $\Delta X = \Delta Y = 0.5$ mm, where an area of 1 mm^2 is described by four measurement points (Figure 3e). In this image, red circles mark wormholes on the wood surface that are not visible in the 3D image.

3. Results

The recorded three-dimensional image was pre-filtered to remove noise caused by the scattering of the laser beam on the wood surface. The image noise was removed using a median filter with a 3×3 matrix structure element. Morphological analysis was performed on the resulting image using an erosion operation. As a result of applying this transformation, the measurement points located directly at the edges of each hole were

directly assigned to the hole (Figure 4a). In this way, the surface area of each hole was increased by the points that formed the edge of the hole. The results of the transformations performed can be seen in the three-dimensional image shown in Figure 4b.

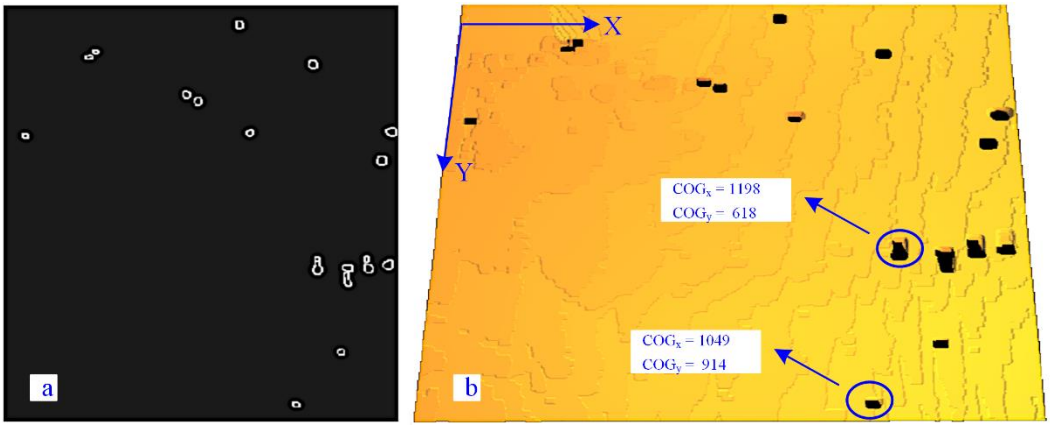

Figure 4. Three-dimensional image of the wood surface: (**a**) regions of the edges detected around each hole; (**b**) three-dimensional surface of the wood with visible wormholes after the filtering operation and hole position identification.

Figure 4 shows the hole regions with precise edges, allowing the x- and y-coordinates of the position of each hole to be identified. The image was described by a grid of points with three coordinates. For a valid wood surface, the z-coordinate of each point describes the actual value of the surface height. For points inside the hole, the height of each point is equal to 0, i.e., Pi (xi, yi, 0). A segmentation based on the height analysis of the points in the three-dimensional image identifies the areas associated with the surface damage.

Regardless of the shape of the defect, the same method of defect localisation was used for regular (circular) and irregular (elongated) holes. A calculation of the centre of gravity of the hole, i.e., the defect visible on the surface, was used. The results of this analysis are presented in Figure 4b. Using this method, it was possible to locate the centre of gravity of a defect visible on the surface, regardless of its shape and dimensions. The coordinates of the position of the centre of each area were determined using the Centre of Gravity (COG) algorithm by analysing a set of points of the hole (Figure 5). By analysing each wormhole separately, the position of the region's centre of gravity was calculated from the x- and y-coordinates of the points P that formed the region.

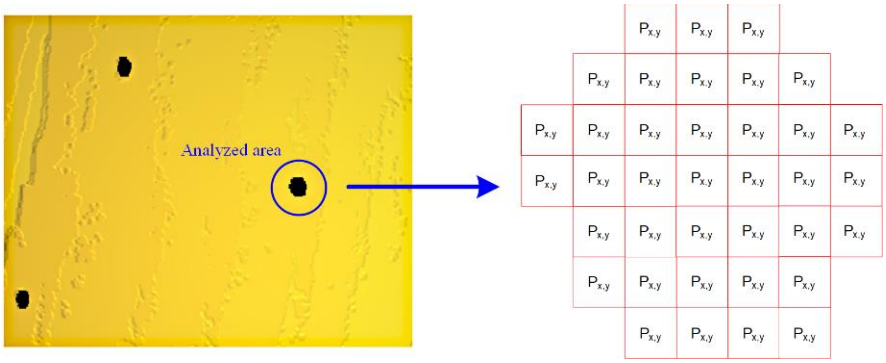

Figure 5. Three-dimensional image of the wood surface: (**a**) wood surface with visible wormhole; (**b**) exemplary description of the wormhole using measurement points.

Using the coordinates of the position of the points that formed the region, the position of the centre of gravity was determined using the following relationship:

$$COG_X = \frac{1}{P}\sum_{i=1}^{P} P_{xi} \quad (4)$$

$$COG_Y = \frac{1}{P}\sum_{i=1}^{P} P_{yi} \quad (5)$$

where:

P—the number of points forming the affected area,
P_{xi}—x-coordinate of point P_i,
P_{yi}—y-coordinate of point P_i.

Based on the three-dimensional image analysis, a set of geometric parameters was determined, describing each area of the detected defect. The perimeter of the defect area was also determined, in addition to three parameters for diameter, i.e., the minimum diameter, maximum diameter, and average diameter measured for the holes. In addition, the perimeter of the defect area and the ovality parameter were calculated for each region. All parameters were determined in the image coordinate system and given in units corresponding to the number of measurement points. Figure 6a shows the location of the damaged areas. Figure 6b shows an example of the measurement results for a sample defect region identified on the wood surface. Each wormhole was described by the coordinates of the location of its centre and parameters describing its area and diameter (Figure 6b). This information was subsequently used to assess the possibility of removal, i.e., cutting out a piece of the surface from the semi-finished product and reusing it in production. The data set prepared above was presented on a synoptic screen for management and machine operators.

$$\text{Area } [\text{mm}^2] = \text{P} \times (\Delta\text{X} \times \Delta\text{Y}) = \text{P} \times (0.125 \times 0.125)\ \text{mm}^2 \quad (6)$$

where:

P—the number of points forming the defect;
ΔX = ΔY = imaging resolution equal to 0.125 mm.

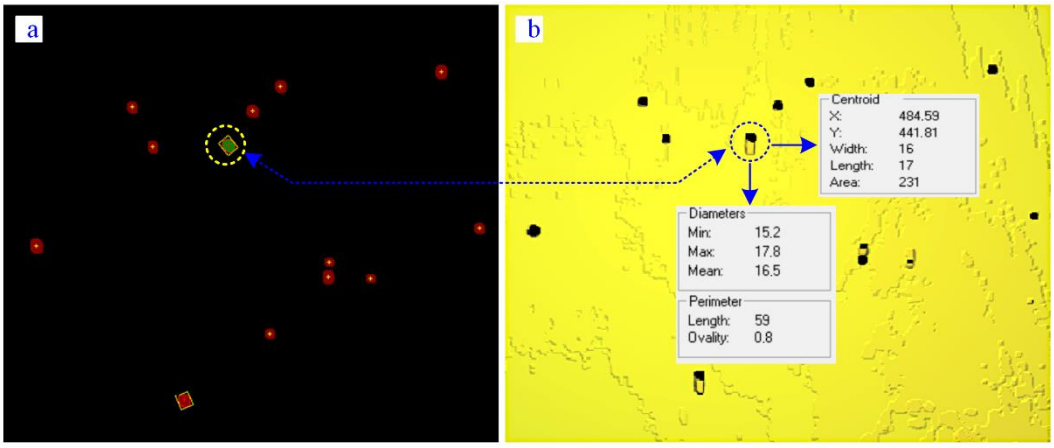

Figure 6. Identified surface defects: (**a**) location and labelling of the defect regions; (**b**) description of the geometric parameters of each defect area.

The hole shape standard model was not considered for the identification of the holes. A mathematical description of a defect area was used, comprising points representing the defect on the surface. These points may lie below the wood surface or have zero height, forming holes. Parameters such as the centre of gravity (COG), defect area, dimensions

(including diameters and perimeter), and ovality were utilised to identify and assess the defects.

4. Discussion

This work proposes a three-dimensional surface imaging system using laser triangulation. A sensor with a resolution of 1536 × 512 has been used. For a field of view (FOVx) of 175 mm, a resolution of 0.125 mm is obtained in the X- and Y-axes. The ability to detect wormholes larger than 1 mm in diameter has been confirmed at this resolution. Increasing the imaging resolution makes it possible to image holes with smaller diameters. To do this, sensors with a higher resolution can be used, i.e., 4096 × 3072 (Automation Technology), which allows imaging with a resolution of ΔX = 175 mm/4096 pixels = 43 μm/pixel. These are theoretical values. Such a solution requires much more computing power and a higher registration frame rate. It would have to be tested in the laboratory and then on an industrial scale in the presence of noise generated by the production line.

The analysis showed that images recorded at a resolution of 0.125 mm/pixel allow a valid assessment of both the detection of wormholes and a complementary analysis of the quality of the surface finish. Images recorded at resolutions of 0.2 and 0.25 mm/pixel can be used to assess the presence of wormholes. However, images recorded at 0.5 mm/pixel resolution should not be used for this inspection task due to insufficient points per 1 mm^2 area.

Laser triangulation imaging allows the determination of geometric parameters describing the surface at the chosen imaging resolution. This type of imaging is unaffected by changes in surface colour caused by changes in wood colour or moisture content. The effect is achieved by using a focused laser beam to illuminate the imaged surface. The 3D image is reproducible regardless of changes in surface colour. A 2D image taken under visible light would reflect colour changes in the wood surface, which in extreme cases would result in the inability to distinguish defects from the surface.

If the inspection task is defined such that any wormholes detected on the surface disqualify the inspected material from further processing, the task is completed when at least one hole is detected. Such material is marked as defective. If the material is sorted into quality categories, it is possible to analyse the distribution of holes when more than one hole is found. This makes it possible to decide whether part of the material should be removed and the remaining part reused in other technological processes.

The surface inspection task can be extended to include measurement of hole diameter and area to evaluate further the suitability of the material for use in another product range. Example measurement results are shown in Figure 5.

By recording a three-dimensional image of the wood surface, it is possible to determine a wide range of parameters describing the quality of the wood surface. This work focuses on detecting specific defects, i.e., wormholes larger than 1 mm in diameter. The system has been designed and manufactured for use at the initial sorting and quality control stage when materials enter production. It removes material with visible damage and sorts it into quality classes. Other wood surface damage classes are also detectable using the proposed configuration. Previous studies have focused on defects related to, among others, fungi, wane, cracks, and dimensional defects [55,56].

In the case of natural cracks, it should be noted that the surface area of such a flaw will be significantly larger than the hole made by the pests. These cracks are also considered surface defects. However, defects can be sorted using either defect area information or defect distribution information. Healthy knots will not be considered a defect because their surface is correct and flat. In the case of knots with a visible perimeter resulting from wood decay processes, this perimeter can also be detected using point analysis and classified as a defect. The discolouration does not affect the evaluation of geometrical defects visible on the wood surface. It remains an open question as to whether to expand the catalogue of defects that can be detected using the proposed configuration.

Analysis of the three-dimensional image makes it possible to identify and locate damaged areas and determine critical geometric parameters. Information on the number of

defects, their distribution, and the damaged area is sufficient to evaluate the material. This information can be used to evaluate semi-finished wood products and manage ongoing production quality. In highly automated productions, such information is crucial for the resulting production efficiency. The consequences of allowing the production of defective semi-finished products may be downtime, damage to machines, or the need to repair manufactured products made of defective elements. Wood quality control systems allow for increased productivity and stable management while maintaining the required product quality. Using parametric defect assessments enables the definition of an acceptable tolerance for each quality indicator. Depending on the intended use of the wood, these tolerances can be adapted by the operators controlling the quality control system. It allows operators to respond rapidly to changes in material grading requirements, enabling flexible control of the process.

The wormhole detection algorithms used belong to classical 3D image analysis methods. The results were satisfactory regarding the possibility of implementation under industrial conditions. AI methods can be investigated and tested as an alternative to classical 3D image analysis methods. No studies related to the use of AI for wormhole detection have been found in the available literature. The use of such techniques and the analysis of their advantages and disadvantages in the dynamic control of quality control process parameters is planned for the following research step.

All tests and image recording were performed at a speed of moving wood relative to the camera and did not exceed 1.5 m/s. Imaging at higher speeds requires cameras with the ability to capture more altitude profiles per second. Solutions that allow users to register profiles with a frequency of up to 200 kHz have already appeared on the market. However, it should be remembered that some of the laser energy illuminating the surface of the wood is absorbed and dissipated. Increasing the frequency of altitude profile recording is associated with a decrease in acquisition time and thus a decrease in the energy recorded on the sensor. It may turn out that the surface of the wood is no longer visible with a frequency of 200 kHz in the 3D image.

Tests should therefore be carried out to confirm the possibility of imaging wood at such frequencies. This is the direction of further work that can be carried out as part of the ongoing research into controlling defects resulting from pests feeding.

Author Contributions: Conceptualisation, A.S., B.L. and A.H.; methodology, A.S., B.L. and A.H.; software, A.S., B.L. and A.H.; validation, B.L., A.S., K.N., Y.N., A.H. and K.H.; formal analysis, B.L., A.S., K.N., Y.N., A.H. and K.H.; investigation, B.L., A.S., K.N., Y.N., A.H. and K.H.; resources, B.L. and A.S.; data curation, B.L., A.S., K.N., Y.N. and K.H.; writing—original draft preparation, A.S. and B.L.; writing—review and editing, B.L., A.S., K.N., Y.N. and K.H.; visualisation, B.L., A.S., K.N., Y.N. and K.H.; supervision, A.S.; project administration, A.S. and B.L.; and funding acquisition, A.S. All authors have read and agreed to the published version of the manuscript.

Funding: This study was financed by the AGH University of Science and Technology in Krakow as part of the IDUB-D11-11155-11167-1178 project.

Informed Consent Statement: Not applicable.

Data Availability Statement: The data presented in this study are available on request from the corresponding author. The data are not publicly available due to privacy.

Conflicts of Interest: The authors declare no conflicts of interest.

References

1. Capecki, Z. Badania Nad Szkodnikami Wtórnymi Jodły i Ich Zwalczaniem. *Pr. IBL* **1982**, *593*, 35–42.
2. Dominik, J.; Starzyk, J. *Atlas Owadów Uszkadzających Drewno*, 1st ed.; Oficyna Wydawnicza MULTICO: Warszawa, Poland, 1998.
3. Kolk, A.; Starzyk, J.R. *Atlas Szkodliwych Owadów Leśnych*; Oficyna Wydawnicza MULTICO: Warszawa, Poland, 1996.
4. Łoziński, J.K. Kwartalnik Wigierskiego Parku Narodowego. 2003. Available online: https://www.wigry.org.pl/kwartalnik/nr12_korniki.htm (accessed on 1 October 2024).
5. Ruz, G.A.; Estévez, P.A.; Ramírez, P.A. Automated Visual Inspection System for Wood Defect Classification Using Computational Intelligence Techniques. *Int. J. Syst. Sci.* **2009**, *40*, 163–172. [CrossRef]

6. Hu, C.; Tanaka, C.; Ohtani, T. Locating and Identifying Sound Knots and Dead Knots on Sugi by the Rule-Based Color Vision System. *J. Wood Sci.* **2004**, *50*, 115–122. [CrossRef]
7. Chen, Y.; Sun, C.; Ren, Z.; Na, B. Review of the Current State of Application of Wood Defect Recognition Technology. *Bioresources* **2022**, *18*, 2288. [CrossRef]
8. Bucur, V. Techniques for High Resolution Imaging of Wood Structure: A Review. *Meas. Sci. Technol.* **2003**, *14*, R91–R98. [CrossRef]
9. Funck, J.W.; Zhong, Y.; Butler, D.A.; Brunner, C.C.; Forrer, J.B. Image Segmentation Algorithms Applied to Wood Defect Detection. *Comput. Electron. Agric.* **2003**, *41*, 157–179. [CrossRef]
10. Jiang, Z.; Liang, Y.; Su, Z.; Chen, A.; Sun, J. Nondestructive Testing of Mechanical Properties of Bamboo–Wood Composite Container Floor by Image Processing. *Forests* **2021**, *12*, 1535. [CrossRef]
11. Faria, J.; Martins, T.; Ferreira, M.; Santos, C. A Computer Vision System for Color Grading Wood Boards Using Fuzzy Logic. In Proceedings of the 2008 IEEE International Symposium on Industrial Electronics, Cambridge, UK, 30 June–2 July 2008; pp. 1082–1087.
12. Yang, Y.; Zhou, X.; Liu, Y.; Hu, Z.; Ding, F. Wood Defect Detection Based on Depth Extreme Learning Machine. *Appl. Sci.* **2020**, *10*, 7488. [CrossRef]
13. He, T.; Liu, Y.; Yu, Y.; Zhao, Q.; Hu, Z. Application of Deep Convolutional Neural Network on Feature Extraction and Detection of Wood Defects. *Measurement* **2020**, *152*, 107357. [CrossRef]
14. Haciefendioglu, K.; Başaga, H.B.; Bulut, M.C.; Kartal, M.E. Automatic Damage Detection on Traditional Wooden Structures with Deep Learning-Based Image Classification Method. *Drv. Ind.* **2022**, *73*, 163–176. [CrossRef]
15. Hu, J.; Yu, X.; Zhao, Y.; Wang, K.; Lu, W. RESEARCH ON BAMBOO DEFECT SEGMENTATION AND CLASSIFICATION BASED ON IMPROVED U-NET NETWORK. *Wood Res.* **2022**, *67*, 109–122. [CrossRef]
16. Sun, P. Wood Quality Defect Detection Based on Deep Learning and Multicriteria Framework. *Math. Probl. Eng.* **2022**, *2022*, 4878090. [CrossRef]
17. Meinlschmidt, P. Thermographic Detection of Defects in Wood and Wood Based Materials. In Proceedings of the 14th International Sumposium of Nondestructive Testing of Wood, Hannover, Germany, 2–4 May 2005; p. 6.
18. Pitarma, R.; Crisóstomo, J.; Pereira, L. Detection of Wood Damages Using Infrared Thermography. *Procedia Comput. Sci.* **2019**, *155*, 480–486. [CrossRef]
19. Pastorino, M.; Randazzo, A.; Fedeli, A.; Salvadè, A.; Poretti, S.; Maffongelli, M.; Monleone, R.; Lanini, M. A Microwave Tomographic System for Wood Characterization in the Forest Products Industry. *Wood Mater. Sci. Eng.* **2015**, *10*, 75–85. [CrossRef]
20. Hislop, G.; Hellicar, A.D.; Li, L.; Greene, K.; Lewis, C.; Meder, R. Microwave Radar for Detection of Resin Defects in *Pinus elliottii* Engelm var *elliottii*. *Holzforschung* **2009**, *63*, 571–574. [CrossRef]
21. Tiitta, M.; Tiitta, V.; Gaal, M.; Heikkinen, J.; Lappalainen, R.; Tomppo, L. Air-Coupled Ultrasound Detection of Natural Defects in Wood Using Ferroelectret and Piezoelectric Sensors. *Wood Sci. Technol.* **2020**, *54*, 1051–1064. [CrossRef]
22. Fleming, M.R.; Bhardwaj, M.C.; Janowiak, J.J.; Shield, J.E.; Roy, R.; Agrawal, D.; Bauer, L.S.; Miller, D.L.; Hoover, K. Noncontact Ultrasound Detection of Exotic Insects in Wood Packing Materials. *Prod. J.* **2005**, *55*, 33–37.
23. Wang, X.; Divos, F.; Pilon, C.; Brashaw, B.K.; Ross, R.J.; Pellerin, R.F. *Assessment of Decay in Standing Timber Using Stress Wave Timing Nondestructive Evaluation Tools: A Guide for Use and Interpretation*; USDA: Washington, DC, USA, 2004.
24. Wei, Q.; Chui, Y.H.; Leblon, B.; Zhang, S.Y. Identification of Selected Internal Wood Characteristics in Computed Tomography Images of Black Spruce: A Comparison Study. *J. Wood Sci.* **2009**, *55*, 175–180. [CrossRef]
25. Choi, B.; Himmi, S.K.; Yoshimura, T. Quantitative Observation of the Foraging Tunnels in Sitka Spruce and Japanese Cypress Caused by the Drywood Termite *Incisitermes Minor* (Hagen) by 2D and 3D X-Ray Computer Tomography (CT). *Holzforschung* **2017**, *71*, 535–542. [CrossRef]
26. McLoughlin, S.; Mays, C. Synchrotron X-Ray Imaging Reveals the Three-Dimensional Architecture of Beetle Borings (Dekosichnus Meniscatus) in Middle–Late Jurassic Araucarian Conifer Wood from Argentina. *Rev. Palaeobot. Palynol.* **2022**, *297*, 104568. [CrossRef]
27. Zhao, G.; Liu, C.; Qiu, Z.; Deng, Z.; Gong, J. 3D Morphology of Internal Defects in Wooden Products Based on Computed Tomography. *Bioresources* **2021**, *16*, 6267–6280. [CrossRef]
28. Ji, A.; Cool, J.; Duchesne, I. Using X-Ray CT Scanned Reconstructed Logs to Predict Knot Characteristics and Tree Value. *Forests* **2021**, *12*, 720. [CrossRef]
29. Fredriksson, M.; Cool, J.; Duchesne, I.; Belley, D. Knot Detection in Computed Tomography Images of Partially Dried Jack Pine (*Pinus Banksiana*) and White Spruce (*Picea Glauca*) Logs from a Nelder Type Plantation. *Can. J. For. Res.* **2017**, *47*, 910–915. [CrossRef]
30. Andreu, J.-P.; Rinnhofer, A. Modeling Knot Geometry in Norway Spruce from Industrial CT Images. In *Image Analysis: 13th Scandinavian Conference, SCIA 2003, Halmstad, Sweden, 29 June–2 July 2003 Proceedings 13*; Springer: Berlin/Heidelberg, Germany, 2003; pp. 786–791.
31. Bhandarkar, S.M.; Faust, T.D.; Tang, M. CATALOG: A System for Detection and Rendering of Internal Log Defects Using Computer Tomography. *Mach. Vis. Appl.* **1999**, *11*, 171–190. [CrossRef]
32. Krähenbühl, A.; Kerautret, B.; Debled-Rennesson, I.; Longuetaud, F.; Mothe, F. Knot Detection in X-Ray CT Images of Wood. In *Advances in Visual Computing: 8th International Symposium, ISVC 2012, Rethymnon, Crete, Greece, 16–18 July 2012, Revised Selected Papers, Part II 8*; Springer: Berlin/Heidelberg, Germany, 2012; pp. 209–218.

33. Wei, Q.; Leblon, B.; La Rocque, A. On the Use of X-Ray Computed Tomography for Determining Wood Properties: A Review. *Can. J. For. Res.* **2011**, *41*, 2120–2140. [CrossRef]
34. Freyburger, C.; Longuetaud, F.; Mothe, F.; Constant, T.; Leban, J.-M. Measuring Wood Density by Means of X-Ray Computer Tomography. *Ann. Sci.* **2009**, *66*, 804. [CrossRef]
35. Manceur, A.M.; Beaulieu, J.; Han, L.; Dutilleul, P. A Multidimensional Statistical Model for Wood Data Analysis, with Density Estimated from CT Scanning Data as an Example. *Can. J. For. Res.* **2012**, *42*, 1038–1049. [CrossRef]
36. Longuetaud, F.; Mothe, F.; Leban, J.-M. Automatic Detection of the Heartwood/Sapwood Boundary within Norway Spruce (Picea Abies (L.) Karst.) Logs by Means of CT Images. *Comput. Electron. Agric.* **2007**, *58*, 100–111. [CrossRef]
37. Skog, J.; Oja, J. Heartwood Diameter Measurements in *Pinus Sylvestris* Sawlogs Combining X-Ray and Three-Dimensional Scanning. *Scand. J. Res.* **2009**, *24*, 182–188. [CrossRef]
38. Johansson, E.; Johansson, D.; Skog, J.; Fredriksson, M. Automated Knot Detection for High Speed Computed Tomography on *Pinus sylvestris* L. and *Picea abies* (L.) Karst. Using Ellipse Fitting in Concentric Surfaces. *Comput. Electron. Agric.* **2013**, *96*, 238–245. [CrossRef]
39. Berglund, A.; Broman, O.; Grönlund, A.; Fredriksson, M. Improved Log Rotation Using Information from a Computed Tomography Scanner. *Comput. Electron. Agric.* **2013**, *90*, 152–158. [CrossRef]
40. Stängle, S.M.; Brüchert, F.; Heikkila, A.; Usenius, T.; Usenius, A.; Sauter, U.H. Potentially Increased Sawmill Yield from Hardwoods Using X-Ray Computed Tomography for Knot Detection. *Ann. Sci.* **2015**, *72*, 57–65. [CrossRef]
41. Rais, A.; Ursella, E.; Vicario, E.; Giudiceandrea, F. The Use of the First Industrial X-Ray CT Scanner Increases the Lumber Recovery Value: Case Study on Visually Strength-Graded Douglas-Fir Timber. *Ann. Sci.* **2017**, *74*, 28. [CrossRef]
42. Belley, D.; Duchesne, I.; Vallerand, S.; Barrette, J.; Beaudoin, M. Computed Tomography (CT) Scanning of Internal Log Attributes Prior to Sawing Increases Lumber Value in White Spruce (*Picea Glauca*) and Jack Pine (*Pinus Banksiana*). *Can. J. For. Res.* **2019**, *49*, 1516–1524. [CrossRef]
43. Gergeľ, T.; Bucha, T.; Gejdoš, M.; Vyhnáliková, Z. Computed Tomography Log Scanning—High Technology for Forestry and Forest Based Industry. *Cent. Eur. For. J.* **2019**, *65*, 51–59. [CrossRef]
44. Gergeľ, T.; Hamza, J.; Ondrejka, V.; Němec, M.; Vanek, M.; Drugdová, J. Radiation Protection of a 3D Computer Tomography Scanning Workplace for Logs—A Case Study. *Sensors* **2023**, *23*, 8937. [CrossRef] [PubMed]
45. Thomas, L.; Mili, L.; Thomas, E.; Shaffer, C.A. Defect Detection on Hardwood Logs Using Laser Scanning. *Wood Fiber Sci.* **2006**, *38*, 696–716.
46. Ondrejka, V.; Gergeľ, T.; Bucha, T.; Pástor, M. Innovative Methods of Non-Destructive Evaluation of Log Quality. *Cent. Eur. For. J.* **2021**, *67*, 3–13. [CrossRef]
47. Sioma, A. Quality Control System of Wooden Flanges Based on Vision Measurement System. *Wood Res.* **2019**, *64*, 637–646.
48. Sioma, A. 3D Imaging Methods in Quality Inspection Systems. In *Photonics Applications in Astronomy, Communications, Industry, and High-Energy Physics Experiments 2019*; Romaniuk, R.S., Linczuk, M., Eds.; SPIE: Bellingham, WA, USA, 2019; p. 91.
49. Jiang, R.; Zhou, X.; Ran, M. 3D Reconstruction and morphology analysis of coarse aggregate using optical laser triangulation and image processing technology. *Road Mater. Pavement Des.* **2022**, *25*, 790–819. [CrossRef]
50. Sioma, A.; Karwat, B. The Use of 3D Imaging in Surface Flatness Control Operations. *Adv. Sci. Technol. Res. J.* **2023**, *17*, 335–344. [CrossRef] [PubMed]
51. Ali, M.A.; Wang, D.; Tao, Y. Active Dual Line-Laser Scanning for Depth Imaging of Piled Agricultural Commodities for Itemized Processing Lines. *Sensors* **2024**, *24*, 2385. [CrossRef] [PubMed]
52. Hauck, J.; Gniado, P. Laser Scan Compression for Rail Inspection. *Sensors* **2024**, *24*, 6722. [CrossRef] [PubMed]
53. Wang, W.; Cai, Y.; Carlson, B.; Poss, M. Quality inspection scheme for automotive laser braze joints. *Int. J. Adv. Manuf. Technol.* **2020**, *106*, 1553–1566. [CrossRef]
54. Sioma, A. Geometry and Resolution in Triangulation Vision Systems. In *Photonics Applications in Astronomy, Communications, Industry, and High Energy Physics Experiments 2020*; Romaniuk, R.S., Linczuk, M., Eds.; SPIE: Bellingham, WA, USA, 2020; p. 33.
55. Sioma, A.; Lenty, B. Detection of Fungal Infections on the Wood Surface Using LTM Imaging. *Appl. Sci.* **2023**, *13*, 490. [CrossRef]
56. Cinal, M.; Sioma, A.; Lenty, B. The Quality Control System of Planks Using Machine Vision. *Appl. Sci.* **2023**, *13*, 9187. [CrossRef]